

Additional methods are available in the online Supporting Material.

## Results

### Visualizing the whole architecture of the mouse biliary tree

In canonical histological analyses of liver sections, bile ducts can be detected as an epithelial tissue with tubular structure, consisting of BECs and being located adjacent to the portal vein (Figure 1A). The entirety of the bile ducts spreads three-dimensionally in the whole liver along with the portal vein and is thus considered the biliary tree. Although several imaging techniques, including resin castings and cholangiography, can be used to broadly capture this tree-like structure, the precise, fine-scale architecture of the peripheral biliary branches remains unknown (14, 15). This prompted us to develop a novel approach to observe the fine three-dimensional (3D) architecture of the mouse biliary tree.

The biliary tract was filled with ink by retrograde injection from the extrahepatic bile duct, and the whole liver was excised from the animal and then soaked in the BABB solution for optical clearing of the tissue. This simple method successfully revealed the precise architecture of the mouse biliary tree at an organ-wide level; in the normal uninjured liver, large diameter tubes run parallel to the portal veins at about a 1:1 ratio, while small diameter tubules intricately branch and wrap around the portal vein to form the biliary plexus (Figures 1B–1F). Immunostaining for the BEC marker cytokeratin 19 (CK19) on sections of liver samples pre-treated with ink injection showed almost complete colocalization of the ink and marker (Figures 1G and 1H). This result

## Hepatology

indicates that the structure observed by the conduit for the ink consistently recapitulates the epithelial tubular architecture constituted by BECs.

## Emergence and expansion of LPCs reflects remodeling of the biliary tree

By using this ink injection strategy, we next asked the question as to whether LPCs in injured liver are connected to the bile duct. Section analysis after ink injection into the biliary tree in the liver of a mouse treated with a toxin, DDC, that typically causes chronic liver injury, showed colocalization of the ink with CK19<sup>+</sup> cells (Figures 2A–2C and Figures S1A–S1D). This indicates that LPCs actually formed tubular structures connected to the pre-existing biliary tree, constituting a contiguous, whole conduit system. This was also the case in all other types of chronic injury models tested, including the CDE, the CCl<sub>4</sub>, and the TAA models (Figures S1E–S1H).

Taking advantage of the newly developed visualization method, we further observed the 3D architecture of the biliary tree in DDC-treated livers and found that the biliary tree dynamically transformed, with its branches being more extended outward to the parenchymal area (Figures 2D–2F). Time-course analysis showed that the tree gradually and contiguously transformed in response to injury (Figure S2). To strengthen this notion, we also developed a 3D imaging technique using 200-µm-thick tissue sections combined with immunostaining and confirmed that there were no biliary marker-positive cells that were separated from the branches (Figure S3). Collectively, these results show that LPCs that have traditionally been defined in histopathological examinations of two-dimensional (2D) liver tissue sections actually emerge as a consequence of the expansion and remodeling of the biliary architecture from the

## Hepatology

viewpoint of 3D histodynamics.

Previous studies have identified several key signaling pathways and molecules that play physiologically relevant roles in regulating LPCs (16). Among them, FGF7 and tumor necrosis factor-like weak inducer of apoptosis (TWEAK) can be regarded as the primary inducers for LPCs, as forced expression of either of these factors in the normal liver can sufficiently induce cells characteristically reminiscent of LPCs, even in the absence of any injury condition (11, 17). As we revealed that LPCs emerge as the consequence of the morphological transformation of the biliary architecture, we re-evaluated the effects of these factors from this new viewpoint. We analyzed the biliary tree following overexpression of FGF7 or TWEAK in the liver by hydrodynamic delivery of the expression plasmid (18, 19). As expected, either of these factors was capable of inducing proliferation of CK19<sup>+</sup> cells, leading to an increase in the CK19<sup>+</sup> area in liver tissue sections when compared with the LacZ-overexpressed control sample (Figures 3A-3E). 3D observation of the biliary architectures in those livers (Figures 3F and 3G) revealed that FGF7 induced increased density of the biliary branches, leading to expansion and parenchymal invasion of the biliary network (Figure 3G). In contrast, TWEAK did not induce apparent transformation of the tubular architecture as revealed by the ink injection (Figure 3F). Together with the section analysis after ink injection (Figures 3H and 3I), the results demonstrate that the mode of action of FGF7 is to induce the morphological transformation of the biliary branches with an intact tubular structure. Notably, TWEAK and FGF7 both induced similar levels of increment in the CK19<sup>+</sup> area in the section analysis (Figure 3E), which appears contradictory to the difference observed in 3D (compare Figures 3F and 3G). In order to manifest and quantitate the possible morphological difference in the biliary architectures resulting from the distinct effects of

#### Hepatology

TWEAK and FGF7, we analyzed the value of (perimeter)<sup>2</sup>/area for all the CK19<sup>+</sup> regions (i.e., cell clusters) in the whole section of each samples. This parameter is expected to become higher when the patterns of the region are more complicated or scattered (Figure 3J, schematic), and does not change upon homothetic transformation. This type of parameters reflecting the ratio of the area and the square of perimeter for objects are often used in studies such as those assessing the shapes of cells, nuclei, wounds and nanowires (20-23). As a result, the value was significantly higher in the FGF7-overexpressed liver compared with those in the LacZ- or TWEAK-overexpressed liver, whereas no significant difference was observed between the values for the latters (Figure 3J). This supports the idea that FGF7 induces changes in the pattern of the CK19<sup>+</sup> area, while the enlargement of the CK19<sup>+</sup> area caused by TWEAK may be rather homothetic. Collectively, the results show that FGF7 has an effect clearly distinct from that of TWEAK in that only the former can induce changes in the architecture of the biliary branches, even though both of them induce cell proliferation.

# Diverse transformations of the biliary architecture corresponding to different types of liver injury

Functioning as the primary center for detoxification and metabolism, the liver processes many kinds of chemicals and toxins and is thus inherently predisposed to incurring a wide variety of damage with distinct etiologies and injury patterns (Figure S4). While several types of liver injury regimens are often arbitrarily and interchangeably employed as models for LPC induction in mice, recent evidence shows that LPCs induced in each model actually show divergent characteristics (4, 24). We therefore compared the

#### Hepatology

response dynamics of the biliary tree in various chronic liver injury models with different causative toxins, and found that distinct architectures were clearly exhibited in response to different injuries (Figures 4A–4H). Interestingly, the architectures seemed to be well adapted for each injury pattern, which can be roughly classified into two types for simplification (Figures 4I and 4J). When hepatocytes, including those in the peri-portal region, were injured, as represented by the DDC and the CDE models, biliary branches intricately split around the portal vein (Figures 4A–4D and 4I). In stark contrast, in the CCl<sub>4</sub> and the TAA models, where zonal metabolizing activity restricts production of toxic metabolites and concomitant hepatocyte death only to the peri-central region, the branches exhibited a characteristic structure that extended in a relatively straight line toward the injured area (Figures 4E–4H and 4J). We used tissue sections to quantify the area of the biliary marker epithelial cell adhesion molecule (EpCAM)-positive cells along the porto-central axis, which revealed that their distribution was significantly more extended towards the central vein in the TAA model compared with that of the CDE model (Figure 4K).

From the 3D observation with the ink, we suspected that the different architectures of the bile ducts corresponding to injury patterns might reflect the difference in their directionality, which is hardly evaluated in accurate and precise ways by the 2D analysis. To test this hypothesis, we utilized the 3D imaging technique with 200-µm-thick tissue sections (Figure 5A and Figure S3) to quantitatively examine the directionality of the biliary branches resulting from the transformation. We skeletonized the branches as filaments, and analyzed the branches as vector sets (Figures 5B and 5C). We calculated the parameter for the directionality (*D*) as shown in Figure 5D. When the branches are directed only in the plane vertical to the radius of the portal vein (represented as "the

## Hepatology

tangential plane"), D becomes 0, and when the branches are completely unidirectional, D becomes 1. In a hypothetical simplified case where the branches expand completely in a random manner with the branch lengths being uniform, the simple theoretical value  $D_{random}$  can be estimated to be around 0.64 as shown in Supplementary Materials and Methods and Figure S5. We then calculated the value of D in the CDE and TAA models as representatives for different injury patterns (Figure 5E). The result showed that in the TAA model the branches were highly directional ( $D = 0.90 \pm 0.02$ ), whereas those in the CDE model are directed nearly at random ( $D = 0.58 \pm 0.02$ ). We also calculated the parameter D' as shown in the Supplementary Materials and Methods to confirm that the approximation of branches to vectors minimally affected the results (see Supplementary Materials and Methods). Combined with the cellular distribution analysis in 2D (Figure 4K), these results indicate that directionality of the transformed branches changes significantly corresponding to the injury patterns (Figures 4I and 4J).

#### Discussions

In this study, we developed and introduced novel methods for delineating the 3-D structure of the biliary tree in the mouse liver, which include: the simple visualization method with the ink injection and optical clearing of the whole liver; the section analysis in combination with ink injection to test the tubular connection; and, the immunostaining and quantitative evaluation protocols for BECs in thick liver sections. By combining these original approaches, we have hereby revealed the hitherto unrecognized fine-scale architecture of the mouse biliary tree under the normal condition, as well as its unprecedented structural dynamics in response to liver injury. Based on the canonical histological observation of liver sections, bile ducts are depicted

## Hepatology

in many textbooks as a simple epithelial tubular structure with clear luminal space located adjacent to the portal vein, constituting a part of the portal triad. Notably, BECs without apparent tubular structure are also observed in the normal liver along the periphery of the portal vein (Figure 1A, arrowheads), but the presence and nature of these cells are often dismissed. Obviously, they should correspond to the biliary plexus that we identified with the 3-D analysis, which branches intricately around the portal vein to form apparently distinct structure from the large diameter bile duct tube running parallel to the portal vein (Figure 1E and 1F). This structural heterogeneity may correspond to the epithelial diversity around the bile ducts (25). Other imaging techniques employed thus far to reveal the 3-D architecutre of the biliary tree, including resin castings and cholangiography (14, 15), did not seem to have sufficient resolution so that they were incapable of capturing and distinguishing these different structures. Thus, our novel methods are advantageous to readily perform precise observation of the complicated and elaborated biliay structure, and should also be useful for studies on the bile duct development as well as pathogenesis of biliary disease models such as polycystic liver disease.

The method with ink injection and that with thick sections are complementary to each other. The former can clarify the large-scale view of the biliary tree at an organ-wide level, but is less amenable to quantitative analysis. In contrast, the latter provides the data on the middle-scale view of the biliary branches that can be subject to quantitative evaluation. In addition, the former detects the biliary tree structure based on the tubular connectivity, while the latter based on the epithelial cellular architecture visualized by staining for marker molecules expressed therein. Combinatorial use of these different types of approaches enables us to conduct comprehensive analyses on the biliary system,

#### Hepatology

covering large aspects of its phenotypes and dynamics.

In liver pathology, LPCs have usually been described as a population distinct from, though related to, BECs, based on their parenchymal location and morphological differences (26, 27). Our present results clearly show that LPCs and BECs together constitute an integral epithelial tubular structure and cannot strictly be distinguished at the histological level, although some phenotypical heterogeneity might still exist among them at the functional levels such as clonogenic activity and differentiation capability. Notably, the expansion of the biliary branches does not necessarily mean that they all arise from the pre-existing BECs; theoretically, they can also continuously arise from neighboring cells by means such as cell type conversion from hepatocytes or differentiation from putative stem/progenitor cells located in the junctional structure between BECs and hepatocytes, or the canal of Hering (28). In fact, recent studies have shown that hepatocytes can convert to biliary epithelial cells under certain types of liver injury conditions, thereby contributing to a part of the ductular reaction (2, 29-31). Nevertheless, our results showing that the biliary tree expands as contiguous structure strongly suggest that such hepatocyte-to-BEC conversion occurs solely adjacent to or near the bile ducts. One possible explanation for this is that hepatocytes beside the bile ducts may have unique characteristics with the ability to convert to BECs. Alternatively, bile ducts or the junctional structure of the canal of Hering may impose some signals that can induce and/or permit conversion of adjacent hepatocytes.

By using the new methods, we also demonstrate that FGF7 and TWEAK have different cellular effects on the biliary epithelium. This further suggests that in response to injuries, the liver actively stimulates multiple signaling pathways with different effects that may coordinately induce the dynamic remodeling of the biliary tree. Regarding the cellular

#### Hepatology

dynamics and mechanisms of the ductular reaction, our findings highlight the need in the future to focus not only on the proliferation or mobility of the cells but also on the morphogenetic aspects of their reaction, such as protrusion of the cells and cell division direction. While our observations in the current study are still static and based on "snapshots" at fixed time points, we expect that future time-lapse analyses of the cellular dynamics, such as those employing intravital live imaging systems, should uncover the active remodeling process of the biliary epithelial architecture.

The novel methods developed in this study enable us to capture the 3D characteristics of the ductular reaction, which appears disordered in 2D sections. Our results showed that the biliary branches exhibited expanded structure with apparent tropism toward the injury area. The dynamic and diverse reconstruction of the biliary architecture corresponding to different types of liver injury may represent an adaptive response of the tissue and should have several physiological advantages. Considering the primary role of the biliary tree as the conduit of bile excretion, its expansion should contribute to ameliorate cholestatic injury conditions. It may also be beneficial in the excretion and elimination of lipophilic toxins and wastes, thereby protecting the liver from sustained damages. Additionally, considering the classical view on LPCs as progenitor cells (1-5) and that the bile ducts themselves have been reported to be a compartment harboring potential stem/progenitor cells in the liver (28, 32), it is possible that the expanded biliary branches can also contribute as the extended source or niche for progenitors that facilitates the local hepatocyte supply and resultant liver regeneration.

With regard to this issue, however, many recent studies using conventional liver disease models in mice have collectively shown that contribution of activated stem/progenitor cells or the biliary compartment to new hepatocytes is usually very limited (3, 4), or even

#### Hepatology

undetectable in some cases, thereby casting doubt on the presence of adult hepatic progenitor cells in the first place (6-8). Perhaps the liver pathologies in these models are not sufficiently severe, so that hepatocytes that are exempt from damage can still extensively proliferate and replenish the lost tissue, making the contribution of the stem/progenitor cells obscure (2, 33, 34). Notably, in the cases of more radical hepatocyte injury models developed in other animals, predominant contribution of the biliary/progenitor compartment has been reported (2, 34, 35). In this regard, our result showing that the biliary branches extend to the peri-central necrotic area in the chronic CCl<sub>4</sub> or TAA models may suggest the possibility that the supply of hepatocytes from biliary/progenitor compartment is spatially restricted to regions only where hepatocytes are subject to persistent and intolerable levels of damage. In addition, it is possible that the extended biliary branches also act as a local scaffold, or a niche, to support and facilitate hepatocyte regeneration from peri-ductal cells by providing juxtacrine or paracrine signaling (8).

In conclusion, our results demonstrate that the liver achieves the diverse remodeling of the biliary architecture corresponding to the nature of injuries, although the mechanism that defines the directionality of the branches still remains to be solved. We propose that the liver can be a prominent model where dynamic epithelial tissue remodeling occurs even in adulthood as an adaptive response against various stress conditions.

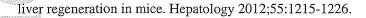
## References

1. Miyajima A, Tanaka M, Itoh T. Stem/Progenitor Cells in Liver Development, Homeostasis, Regeneration, and Reprogramming. Cell Stem Cell 2014;14:561-574.

## Hepatology

- 2. Michalopoulos GK. The liver is a peculiar organ when it comes to stem cells. Am J Pathol 2014;184:1263-1267.
- 3. Espanol-Suner R, Carpentier R, Van Hul N, Legry V, Achouri Y, Cordi S, Jacquemin P, et al. Liver progenitor cells yield functional hepatocytes in response to chronic liver injury in mice. Gastroenterology 2012;143:1564-1575 e1567.
- 4. Rodrigo-Torres D, Affo S, Coll M, Morales-Ibanez O, Millan C, Blaya D, Alvarez-Guaita A, et al. The biliary epithelium gives rise to liver progenitor cells. Hepatology 2014.
- Sackett SD, Li Z, Hurtt R, Gao Y, Wells RG, Brondell K, Kaestner KH, et al. Foxl1 is a marker of bipotential hepatic progenitor cells in mice. Hepatology 2009;49:920-929.
- 6. Yanger K, Knigin D, Zong Y, Maggs L, Gu G, Akiyama H, Pikarsky E, et al. Adult hepatocytes are generated by self-duplication rather than stem cell differentiation. Cell Stem Cell 2014;15:340-349.
- 7. Schaub JR, Malato Y, Gormond C, Willenbring H. Evidence against a Stem Cell Origin of New Hepatocytes in a Common Mouse Model of Chronic Liver Injury. Cell Rep 2014;8:933-939.
- 8. Tarlow BD, Finegold MJ, Grompe M. Clonal tracing of Sox9+ liver progenitors in oval cell injury. Hepatology 2014.
- 9. Lowes KN, Brennan BA, Yeoh GC, Olynyk JK. Oval cell numbers in human chronic liver diseases are directly related to disease severity. Am J Pathol 1999;154:537-541.
- 10. **Ishikawa T, Factor VM**, Marquardt JU, Raggi C, Seo D, Kitade M, Conner EA, et al. Hepatocyte growth factor/c-met signaling is required for stem-cell-mediated

#### Hepatology



- 11. Takase HM, Itoh T, Ino S, Wang T, Koji T, Akira S, Takikawa Y, et al. FGF7 is a functional niche signal required for stimulation of adult liver progenitor cells that support liver regeneration. Genes Dev 2013;27:169-181.
- Yeoh GC, Ernst M, Rose-John S, Akhurst B, Payne C, Long S, Alexander W, et al. Opposing roles of gp130-mediated STAT-3 and ERK-1/ 2 signaling in liver progenitor cell migration and proliferation. Hepatology 2007;45:486-494.
- 13. Sekiya S, Suzuki A. Intrahepatic cholangiocarcinoma can arise from Notch-mediated conversion of hepatocytes. J Clin Invest 2012;122:3914-3918.
- 14. Sparks EE, Perrien DS, Huppert KA, Peterson TE, Huppert SS. Defects in hepatic Notch signaling result in disruption of the communicating intrahepatic bile duct network in mice. Dis Model Mech 2011;4:359-367.
- Ernst TM, Schwinge D, Raabe N, Daubmann A, Kaul MG, Adam G, Schramm C, et al. Imaging of the murine biliopancreatic tract at 7 tesla: Technique and results in a model of primary sclerosing cholangitis. J Magn Reson Imaging 2013.
- 16. Itoh T, Miyajima A. Liver regeneration by stem/progenitor cells. Hepatology 2014;59:1617-1626.
- Jakubowski A, Ambrose C, Parr M, Lincecum JM, Wang MZ, Zheng TS, Browning B, et al. TWEAK induces liver progenitor cell proliferation. J Clin Invest 2005;115:2330-2340.
- 18. Zhang G, Budker V, Wolff JA. High levels of foreign gene expression in hepatocytes after tail vein injections of naked plasmid DNA. Hum Gene Ther 1999;10:1735-1737.
- 19. Wooddell CI, Reppen T, Wolff JA, Herweijer H. Sustained liver-specific

#### Hepatology

transgene expression from the albumin promoter in mice following hydrodynamic plasmid DNA delivery. J Gene Med 2008;10:551-563.

- Wang Y, Filius A, Zhao C, Passe SM, Thoreson AR, An KN, Amadio PC.

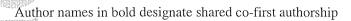
  Altered median nerve deformation and transverse displacement during wrist movement in patients with carpal tunnel syndrome. Acad Radiol 2014;21:472-480.
- 21. Uchihara T, Iwabuchi K, Funata N, Yagishita S. Attenuated nuclear shrinkage in neurons with nuclear aggregates--a morphometric study on pontine neurons of Machado-Joseph disease brains. Exp Neurol 2002;178:124-128.
- 22. Cardinal M, Eisenbud DE, Armstrong DG. Wound shape geometry measurements correlate to eventual wound healing. Wound Repair Regen 2009;17:173-178.
- 23. Fernandez-Garrido S, Kaganer VM, Hauswald C, Jenichen B, Ramsteiner M, Consonni V, Geelhaar L, et al. Correlation between the structural and optical properties of spontaneously formed GaN nanowires: a quantitative evaluation of the impact of nanowire coalescence. Nanotechnology 2014;25:455702.
- Boulter L, Govaere O, Bird TG, Radulescu S, Ramachandran P, Pellicoro A, Ridgway RA, et al. Macrophage-derived Wnt opposes Notch signaling to specify hepatic progenitor cell fate in chronic liver disease. Nat Med 2012;18:572-579.
- 25. Isse K, Lesniak A, Grama K, Maier J, Specht S, Castillo-Rama M, Lunz J, et al. Preexisting epithelial diversity in normal human livers: a tissue-tethered cytometric analysis in portal/periportal epithelial cells. Hepatology 2013;57:1632-1643.
- Fausto N. Liver regeneration and repair: hepatocytes, progenitor cells, and stem cells. Hepatology 2004;39:1477-1487.
- 27. Roskams TA, Theise ND, Balabaud C, Bhagat G, Bhathal PS, Bioulac-Sage P,

## Hepatology

- Brunt EM, et al. Nomenclature of the finer branches of the biliary tree: canals, ductules, and ductular reactions in human livers. Hepatology 2004;39:1739-1745.
- 28. Kordes C, Haussinger D. Hepatic stem cell niches. J Clin Invest 2013;123:1874-1880.
- 29. Yanger K, Zong Y, Maggs LR, Shapira SN, Maddipati R, Aiello NM, Thung SN, et al. Robust cellular reprogramming occurs spontaneously during liver regeneration. Genes Dev 2013;27:719-724.
- 30. Sekiya S, Suzuki A. Hepatocytes, rather than cholangiocytes, can be the major source of primitive ductules in the chronically injured mouse liver. Am J Pathol 2014;184:1468-1478.
- 31. Tarlow BD, Pelz C, Naugler WE, Wakefield L, Wilson EM, Finegold MJ, Grompe M. Bipotential Adult Liver Progenitors Are Derived from Chronically Injured Mature Hepatocytes. Cell Stem Cell 2014.
- Furuyama K, Kawaguchi Y, Akiyama H, Horiguchi M, Kodama S, Kuhara T, Hosokawa S, et al. Continuous cell supply from a Sox9-expressing progenitor zone in adult liver, exocrine pancreas and intestine. Nat Genet 2011;43:34-41.
- Fausto N, Campbell JS. The role of hepatocytes and oval cells in liver regeneration and repopulation. Mech Dev 2003;120:117-130.
- 34. Choi TY, Ninov N, Stainier DY, Shin D. Extensive conversion of hepatic biliary epithelial cells to hepatocytes after near total loss of hepatocytes in zebrafish.

  Gastroenterology 2014;146:776-788.
- 35. He J, Lu H, Zou Q, Luo L. Regeneration of liver after extreme hepatocyte loss occurs mainly via biliary transdifferentiation in zebrafish. Gastroenterology 2014;146:789-800 e788.

## Hepatology



## Acknowledgments

We thank Drs. Yuichiro Arima and Hiroki Kurihara for advice on ink injection and tissue clearing methods, and Dr. Tetsuya J. Kobayashi for comments on image data quantification. We also thank members of the Miyajima lab for helpful discussions and advice. The TROMA-III developed by Dr. Rolf Kemler was obtained from the Developmental Studies Hybridoma Bank developed under the auspices of the NICHD and maintained by The University of Iowa, Department of Biology, Iowa City, IA 52242.

## Hepatology

## Figure legends

Number of figures: 5

Number of Supplementary figures: 5

**Figure 1** A novel approach for visualizing the fine-scale 3D architecture of the mouse biliary tree.

(A) A liver section immunostained with biliary marker CK19. Arrowheads show CK19<sup>+</sup> cells without apparent tubular structure. PV, portal vein; CV, central vein; BD, bile duct. (B) Harvested liver without any treatment. (C–E) Architecture of the biliary tree (fine black structure) visualized by using the method developed in this study. GB, gall bladder. (F) Model for the architecture of the biliary tree. The green shows the bile ducts, and the pink shows the portal vein. (G and H) Immunostaining for CK19 (green) on a tissue section of a liver whose biliary tree was filled with ink. Fluorescence image and bright field image are merged. Black ink is colocalized with CK19<sup>+</sup> cells. Scale bars: 100 μm in (A, E, G, and H).

Figure 2 The liver dynamically transforms the biliary tree in response to chronic injury.

(A–C) Immunofluorescent staining for CK19 (green) on a section of the DDC-treated liver whose biliary tree was filled with ink. White dashed lines outline the portal vein. (C) The same field as (B) without the fluorescent image. The black ink is colocalized with CK19<sup>+</sup> cells (arrowheads). The brown particles are the porphyrin that accumulates along with the toxic injury by DDC. The color tone is adjusted to emphasize the contrast between the ink and the porphyrin (see also Figures S1A, S1C and S1D). (D–F)

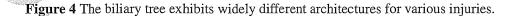
#### Hepatology

Architecture of the biliary tree visualized with ink (black) in the DDC-treated liver (D and E) and its schematic model (F). Scale bars: 100 µm in (A–E).

Figure 3 Different effects of FGF7 and TWEAK on the biliary epithelium.

(A–C) Immunofluorescent staining for CK19 (green) and the proliferation marker Ki67 (red) on tissue sections of the livers where LacZ (A), TWEAK (B). or FGF7 (C) was overexpressed. Blue shows nuclei. (D) Quantification of the proliferation of BECs in the liver upon overexpression of LacZ, TWEAK, or FGF7. Percentages of Ki67<sup>+</sup> cells in CK19<sup>+</sup> cells calculated by cell numbers are shown. (E) Percentages of CK19<sup>+</sup> area per the entire liver section area were calculated for the livers where LacZ, TWEAK, or FGF7 was overexpressed. (F and G) Architecture of the biliary tree in the livers upon overexpresson of TWEAK (F) or FGF7 (G). Note that the branches increase intricately in the FGF7-overexpressed liver. (H and I) Immunofluorescent staining for CK19 (green) on the sections of the livers upon overexpression of TWEAK (H) or FGF7 (I), whose biliary tree was filled with ink. White dashed lines outline the portal vein. The black ink is colocalized with CK19<sup>+</sup> cells, including those distant from the portal vein in the FGF7 overexpressed liver (arrowheads). (J) The value of (perimeter)<sup>2</sup>/area was calculated for all the CK19<sup>+</sup> regions in the whole section of the livers with LacZ, TWEAK, or FGF7 overexpression. Schematic (left) shows hypothetical area patterns for low and high values of (perimeter)<sup>2</sup>/area. Scale bars: 100  $\mu$ m. n = 5 mice for each group in (D, E and J). \*\*P < 0.01; \*\*\*P < 0.001; N.S., not significant. Error bars represent SEM.

## Hepatology



(A-H) Architecture of the biliary tree in liver injury models caused by DDC (A and B), CDE (C and D), CCl<sub>4</sub> (E and F), and TAA (G and H). Scale bars, 100 µm. (I and J) Schematic models for the biliary architectures. Top panels depict a cross-sectional view representing the injury pattern (reddish area) deduced from the histological analyses shown in Figure S4, and the branching pattern of the biliary branches (green) based on the observations shown in the panels A-H. Lower panels show 3D models for the expanded biliary branches around the portal vein (blue box) and in relation to the central vein (purple box; gray zone represents injury area). PV, portal vein; CV, central vein. (I) Biliary branches split intricately around the portal vein; (J) biliary branches are directed to the injured areas. (K) Proportion of biliary marker EpCAM<sup>+</sup> area in each zone from the portal vein to the central vein (1 to 10, x-axis) in the CDE and the TAA models were calculated. The left panel shows immunostaining for EpCAM (green) and tissue autofluorescence (magenta) used for identification of PV and CV. Scale bar, 100 um. Y values were normalized for each mouse so that each graph area correlates with the proportion of total EpCAM<sup>+</sup> cells in the whole section. n = 3 mice  $\times$  10 fields for each group. Error bars represent SEM.

Figure 5 Directionality of the biliary branches shows different patterns corresponding to injury types.

(A) 3D appearance of the reconstructed biliary branches. White shows the staining for CK19 and pink shows the portal vein (see Supplementary Materials and Methods for information on the reconstruction). Scale bar, 50 µm. (B) 3D image of vector extraction

#### Hepatology

method. Green shows the skeletonized biliary branches. Note that the sum of the minute vectors tracing the branches equals the vector from the starting point to the end. (C) Schematic vector extraction method. Green shows the biliary branches and the orange box represents the region of interest (ROI; see Supplementary Materials and Methods). PV, portal vein. (D) Parameter D was calculated for directionality. Simple theoretical values for the parameter D in possible distinctive cases are shown. (E) The value of D was calculated for the CDE and TAA models. Orange dashed lines show simple theoretical values for each indicated case shown in (D). n = 3 mice, total of 17 fields for each group. Error bars represent SEM.

Figure S1 Ink colocalizes with biliary marker-positive cells in various injury models.

(A) Tissue section of a DDC-treated liver immunostained for CK19 (purple). Brown particles are porphyrin, which accumulate along with the toxic injury by DDC. LPCs emerge as ectopic biliary marker positive cells. PV, portal vein; CV, central vein. (B) If LPCs are connected to the pre-existing bile duct (BD), the ink injected in the bile duct reaches these cells (upper model), and if they are not connected, the ink does not reach (lower model). (C–H) Tissue sections of liver injury models with their biliary trees filled with ink. PV, portal vein; CV, central vein. (C and D) A DDC liver immunostained with CK19 (green) (C) and the same image merged with far-red autofluorescence showing porphyrin (red) (D). (E) A CDE liver immunostained with the biliary marker EpCAM. (F) Repetitive CCl<sub>4</sub> injection model immunostained with CK19 (yellow). (G) Liver treated with TAA for 4 wk immunostained for CK19 (red) and collagen (green). Note that ectopic CK19<sup>+</sup> cells spread toward the collagen fiber in the damaged region and that the ink colocalized with these cells (inset). (H) A liver treated with TAA for 8

## Hepatology

wk immunostained for CK19 (green). Scale bars: 100 μm.

Figure S2 Time-course analysis with ink in a DDC liver.

Architectures of the biliary tree (A–C) and sections (D–F) of the liver treated with DDC for 3 (A and D), 5 (B and E), and 8 wk (C and F). The biliary tree was filled with black ink. Sections were immunostained for CK19 (green). Note that CK19<sup>+</sup> cells gradually spread and the ink colocalizes with these cells, showing that these are connected to the pre-existing bile ducts. Brown bodies are porphyrin (Figures S1A, S1C and S1D). Dashed lines outline the portal vein. Scale bars: 100 μm.

Figure S3 3D reconstruction of the biliary branches with 200-μm sections.

Representative 3D reconstruction with confocal images of a 200-μm section of a sample of CDE liver injury model is shown. Example of optical slices is shown. White shows staining for CK19 and blue shows nuclei stained with Hoechst. The top left shows an X-Y plane (pink plane in the schematic), the top right shows a Y-Z plane (yellow plane in the schematic), and the bottom shows an X-Z plane (light blue in the schematic). Yellow lines show intersections. For the X-Z plane, Y-stack projection with the width indicated by the light blue double-headed arrow is shown. The red arrows point the same cells in the three different planes. The red point in the schematic indicates the position of the cells. Note that the point indicated with the red arrow appears separated from the biliary tree in the X-Y plane, but the X-Z plane reveals that it is in fact connected. Scale bar: 50 μm.

#### Hepatology